Journal of Network and Computer Applications 140 (2019) 23–39

Contents lists available at ScienceDirect

Journal of Network and Computer Applications

journal homepage: www.elsevier.com/locate/jnca

Optimal location of supplementary node in UAV surveillance system

Yue Li, Yongmin Zhang, Lin Cai *

Department of Electrical and Computer Engineering, University of Victoria, Canada

ARTICLE INFO

Keywords:
UAV
Monitoring quality
Surveillance system
Deployment triangle
Min-max problem

ABSTRACT

Given the maturity of Unmanned Aerial Vehicle (UAV) technologies, UAVs have been widely used in many areas such as surveillance system. Thanks to the UAV's high mobility, not only the dynamic coverage is now achievable for surveillance systems but also the cost of building (thermal-)camera towers is reduced. The UAV surveillance system includes a UAV mesh network providing seamless monitoring. The target will be tracked down to a warning area which is a triangle formed by the three closest UAVs. A new supplementary UAV is proposed to be deployed inside the warning area to achieve a better monitoring quality. In this paper, we identify the best location of the supplementary UAV by minimizing the maximum service distance in an acute triangle. A closed-form solution is derived for the isosceles acute triangle. For arbitrary acute triangles, a real-time algorithm with low complexity, i.e., the equal service distance (ESD) algorithm, is proposed. Simulation results show that the proposed ESD algorithm can reduce the maximum service distance by up to 35.71%, 15.91%, and 21.74% compared to the incenter, circumcenter, and centroid, respectively. The optimality of the proposed approach is then validated by comparing with the exhaustive search. More simulations considering network dynamics are performed and the impacts of UAV's speed and processing time on monitoring quality are revealed.

1. Introduction

The technologies of Unmanned Aerial Vehicle (UAV) became mature recently. They are light, flexible and have a longer battery life than ever before (Saha et al., 2011), and thus enable the in-depth reconnaissance and surveillance of major incidents, such as uncontrolled emissions of liquid or gaseous contaminants in the cases of volcanic eruptions, wildfires, industrial incidents, crimes, and terrorist attacks. The use of UAV systems for monitoring targets in possible incident areas can greatly facilitate the tasks in police departments, fire brigades, and other homeland security organizations (Daniel and Wietfeld, 2011), (Lilien et al., 2014).

There are two operating stages in the UAV surveillance system. In the first stage, multiple UAVs fly in the mid-air to monitor the incoming incidents, and each of them monitors a certain area. They also interact with each other to ensure good coverage. Because the occurrences of incidents have a low frequency, considering the power consumption and other maintenance costs, it may not be worthy to deploy many UAVs flying simultaneously and waiting for the random incident. Therefore, forming a sparse UAV surveillance mesh network maximizing the monitoring area, i.e, using a limited number of UAVs to provide the maximized coverage, is the guideline of the first-stage UAV deployment.

Given the purpose of the first-stage UAV deployment, the topology plays an important role. An appropriate topology of UAVs helps to achieve a better performance in terms of coverage and cost (Li et al., 2017). Given the fact that the hexagonal mesh topology maximizes the coverage, it is desirable to be used in the first-stage UAV deployment. Once an incident happens, the target can be tracked down to an area formed by the nearest three UAVs. In the hexagonal mesh topology, for any location, the nearest three UAVs forms an equilateral triangle as shown in Fig. 1 (a). Because the incident is inside this triangle, in this paper, we denote this triangle as the warning area, i.e., the area needs to pay extra attention to.

However, given practical issues including geographical constraints, obstacles, and other possible factors like wind, it is difficult for the first-stage UAV mesh network to maintain the perfect hexagonal mesh topology. It also leads to in-equilateral but likely acute triangular warning areas as shown in Fig. 1 (b). Besides, it is still possible for the surveillance system to set different monitoring qualities in different parts of the monitoring area. This makes the first-stage UAV mesh network become denser in the high-quality monitoring area and sparser in other areas, which also results in the in-equilateral warning areas. All of these issues motivate us to design the proposed algorithm to find the optimal location for the new supplementary UAV in an arbitrary acute triangle.

* Corresponding author.
E-mail addresses: liyue331@uvic.ca (Y. Li), ymzhang.zju@gmail.com (Y. Zhang), cai@ece.uvic.ca (L. Cai).

https://doi.org/10.1016/j.jnca.2019.05.006
Received 5 November 2018; Received in revised form 27 April 2019; Accepted 8 May 2019
Available online 15 May 2019

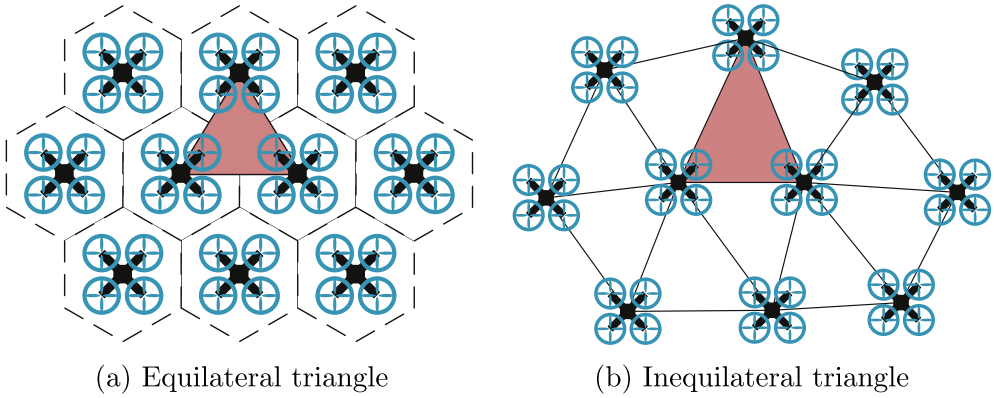

Fig. 1. A triangle warning area.

When a warning area is identified, the surveillance system shall respond quickly and enter the second stage, where it can monitor the area more closely. The first-stage UAV mesh network is sparsely deployed to save the cost, so it may not be sufficient to satisfy the requirement of monitoring quality inside the warning area. Also, because the surveillance tasks in other areas should be maintained, a new supplementary UAV will be sent to the warning area to support the surveillance tasks. Monitoring inside the warning area is critical, and thus the point with the worst monitoring quality, i.e., the worst point, greatly affects the performance of the surveillance system because it determines the existence of blind spots. In this paper, we optimize the location of the newly added UAV in the warning area to improve the monitoring quality to the worst point.

Typically, the monitoring quality depends on the distance, i.e., the distance from the camera mounted on a UAV to the target. If we define the monitoring quality as the resolution of the target in an image or a video, the shorter the distance, the better the quality, especially for thermal cameras. Considering the importance of target monitoring, e.g., tracking down criminals and some severe industrial incidents, we want to ensure that no matter where the target is, the monitoring quality can be guaranteed to be above a certain threshold, i.e, the maximum service distance is below a certain threshold. Even though it may be less likely to see the target in some specific areas, as long as the probability is not zero, we need to consider these areas with the same criteria. Therefore, in this paper, we need to consider every location inside the warning area with equal priority.

Given the equal priority on every location, and the fact that a target is always monitored by the nearest UAV, the problem can be converted to minimizing the longest monitoring distance inside an acute triangle determined by three nearest UAVs in the mesh. The location of the target varies time by time and the tracked target may be moving constantly, so the first-stage UAV swarm may move around an area or along a trace for the optimal coverage. For example, a UAV mesh surveillance network may be moving along an important vehicle to monitor all the potential threats within a one-kilometer radius. As a result, each triangular warning area in the mobile mesh backbone has a dynamic shape and the supplementary UAV should be added to the optimal location which is also time-varying. Hence, a real-time algorithm with low complexity is required to quickly find the optimal location for the newly added UAV given the changing topology.

Besides the UAV surveillance system, similar geometry problems may be raised in other fields as discussed in Sec. 6. Without losing generality, we denote each UAV as a service node and define the distance from a certain location to the nearest UAV as the service distance. The main contributions of this paper are summarized as follows:

- Considering the two-stage UAV surveillance system, a min-max optimization problem is formulated to minimize the longest service distance in an arbitrary acute triangle.
- For the newly added service node, the closed-form expression of the optimal location within an isosceles acute triangle is derived.
- A real-time algorithm with low complexity, i.e., the equal service distance (ESD) algorithm, is proposed to find the optimal location of the new service node within an arbitrary acute triangle.
- Comparisons with the exhaustive search and triangle's existing centers, including incenter, circumcenter, and centroid, are conducted. By simulations, the optimality of the proposed approach is validated and the impacts of UAV's speed and processing time on the performance are investigated.

The rest of paper is organized as follows. In Sec. 2, the related work is described. Sec. 3 presents the system model and problem formulation. The optimal location of the new service node in an isosceles triangle is theoretically derived in Sec. 4.1. The non-isosceles case is then studied in Sec. 4.2. Simulation and Verification are provided in Sec. 5, followed by possible future works and the concluding remarks in Sec. 6.

2. Related work

The use of UAV in the surveillance system has been studied extensively. HAWK, a programmable mini unmanned helicopter armed with a wireless sniffer, was proposed and implemented in (Liu et al., 2014) to conduct surveillance and localization tasks. In (Nigam et al., 2012), multiple UAVs cruise in a target area following optimized trajectories and thus minimize the maximum uncovered time duration of each cell. A feasible distribution of the UAV swarm to properly cover the target area and the trajectory for each UAV to reach the surveillance location were proposed in (Saska et al., 2016). A novel metric to depict the quality of UAVs' deployment, i.e., the deployment entropy, was introduced in (Li et al., 2017), and different deployments were evaluated accordingly. Most of the existing work focused on how to achieve better surveillance coverage while minimizing the number of UAVs, such as (Zorbas et al., 2016), which is the first stage described in Sec. 1.

The UAV surveillance system shares some similarities with the mobile sink in the wireless sensor network (WSN). The main purpose of introducing mobile sinks is to balance energy consumption. Routing methods and data collection strategies were proposed in (Alkesh et al., 2011; Yun and Xia, 2010; Luo et al., 2006; Xu et al., 2010; Abo-Zahhad et al., 2015; Pan et al., 2005) to increase the lifetime of the network. The trade-off between energy saving and traffic delay was analyzed in (Chatzigiannakis et al., 2008). UAVs' topology was kept stable by the gateway selection in (Luo et al., 2015). We also find the similarity of the UAV surveillance system to other UAV's applications, such as the coverage problem in the cellular network (Li and Cai, 2017).

(Alzenad et al., 2017), (Bor-Yaliniz et al., 2016), and (Mozaffari et al., 2016a) focused on maximizing the number of covered users (Tuna et al., 2014). used a team of UAVs in the post-disaster scenario. The interference and backhaul constraints were considered in (Mozaffari et al., 2016b) and (Kalantari et al., 2017), respectively, and users' energy consumption was further optimized in (Mozaffari et al., 2016c) and (Mozaffari et al., 2017). In both of the UAV surveillance system and other UAV-related systems, many existing works can be applied to the first stage of the surveillance system introduced in Sec. 1, but none of them can guide the procedure of the second stage.

In this paper, we focus on the second stage of the UAV surveillance system and optimize the location of the newly added UAV within a triangular warning area. By using the general concept, i.e., service nodes, instead of UAVs, the problem can be mathematically abstracted as finding the optimal location to add a point inside a triangle, which is similar to the facility location problem. In the past decades, the facility location problem had been extensively studied based on different objectives. Most of them are minimizing the sum of the transportation costs from one point to multiple destinations, which is known as the Fermat problem (Tellier, 1972), the Weber problem (Weber, 1929), and the attraction-repulsion problem (Tellier, 1993) according to different definitions of the transportation cost, respectively. Different from these classic problems, we aim to minimize the maximum service distance from any point inside the triangle to its nearest service node, rather than that between two service nodes.

The operation cost of a service node was then considered with the objective of minimizing the overall cost. Depending on whether a service node has limited capacity, the problem can be classified as capacitated and uncapacitated cases (Mirchandani and Francis, 1990). In (Gendron et al., 2017) and (Krishnaswamy and Sviridenko, 2016), the two-level and multi-level uncapacitated facility location problem were studied, respectively. A linear programming-based algorithm was proposed for capacitated case in (An et al., 2017), the financial costs and carbon emission were further considered in (Harris et al., 2014). Instead of assuming fixed sets of locations (or candidates of locations) for facilities and clients in the existing works, we target the scenario where the location of the newly added service node is selected from a continuous plane. The worst point, which can be considered as the client in capacitated/uncapacitated facility location problems, may change according to the different locations of the new service node.

3. System model

3.1. Preliminary

As shown in Fig. 1, once the warning area is determined, a new supplementary UAV, i.e., a new service node, will try to keep staying at the optimal location within the area regardless of the change of topology. The new service node updates its location periodically. We define one period as a slot. At the beginning of each slot, the optimal location is updated according to the latest topology of the mesh. The new service node moves to the updated location directly after the calculation and stays until the next slot. Due to the altitude regulation of UAV system and complex terrain in low altitude area, the UAV surveillance system is likely to operate at an altitude lower than 120 m (the maximum altitude (FAA, 2016)) but still high enough to avoid most obstacles. For simplicity, we assume all the UAVs in the surveillance system have the same altitude.

Given the same altitude, the plane formed by the UAVs is parallel with the ground. We can either project all the UAVs to the ground (where targets are) or project all possible targets to the UAV plane. It is because no matter how we project, the projected longest service distance always represents the longest service distance in reality. Minimizing the projected maximum service distance can help us to achieve the same purpose but the objective is simplified to improve the monitoring/service quality of the worst point inside a 2-D triangle area. The

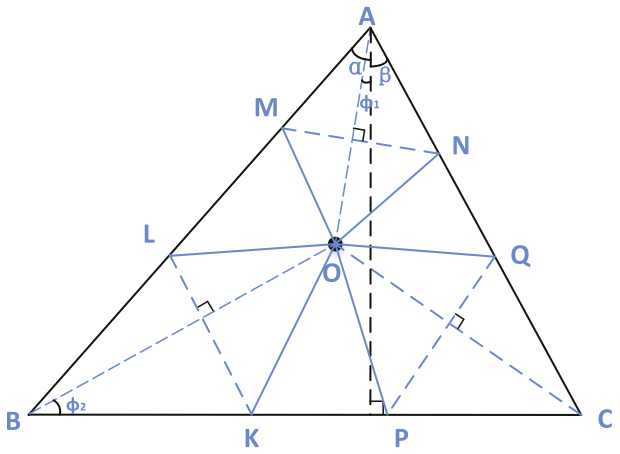

Fig. 2. A triangle formed by three existing service nodes.

monitoring/service quality is determined by the service distance, i.e., the shorter the distance, the better the quality. We only focus on the acute triangle in this paper, and a monitoring target selects the service node based on the shortest service distance.

The first-stage UAVs and supplementary UAVs have different tasks, i.e., coverage and intensive monitoring, respectively. In this paper, we assume that the warning area will only be identified by the first-stage UAV mesh network, and the supplementary UAV will not participate in forming new warning areas. One supplementary UAV will never be selected as the nearest service node by the targets on different warning areas. Therefore, no matter how the supplementary UAV changes its location inside a warning area, the topology outside this warning area will not be changed. If we have multiple warning areas, each warning area will be added a supplementary UAV, and they work independently.

To find out the worst point and the longest service distance, we use Fig. 2 as an example. The point O represents the newly added supplementary UAV, and the points A, B, C represent the existing UAVs in the first-stage surveillance system forming the warning area. Given α, β, the angles of the altitude through vertex A and two sides $\|AB\|, \|AC\|$, the length of $\|AB\|$, a triangle $\triangle ABC$ can be determined. Any point O inside $\triangle ABC$ can be denoted as a function of ϕ_1 and ϕ_2. ϕ_1 denotes the angle of segment OA to the altitude. ϕ_2 denotes the angle between segment OB and BC. Given the principle of service node selection, the triangle area is divided into several Voronoi cells, and dashed line segments MN, LK, and QP are the cell edges. Voronoi cells are obtained by partitioning the area into regions based on the distance to service nodes, and each corresponding region (cell) consisting of all points closer to that service node than to any other. In Fig. 2, $\triangle AMN$, $\triangle BLK$, $\triangle CPQ$, and the hexagon $MNQPKL$ are four Voronoi cells. For the monitoring target in a Voronoi cell, the service node in the same cell can provide the minimum service distance. For example, for any target in $\triangle AMN$, point A is the closest service node. Other dashed line segments like AO, BO, and CO are auxiliary lines representing how we obtain these Voronoi edges. For example, we obtain the edge LK by drawing the mid-perpendicular line of OB.

It is obvious that $\max(\|OM\|, \|ON\|) \geq \|OX\|$, where X is any point on MN. Similar observations can be found on LK and QP as well. Therefore, we can conclude that all the vertexes of Voronoi cells are candidates of the worst point because one of them lead to the longest service distance. As shown in Fig. 2, there are 6 candidate points, i.e., M, L, K, P, Q, and N. They are on sides of the triangle and are defined as on-boundary vertexes.

Besides that, in some cases, two adjacent vertexes on the triangle's boundary may converge to one vertex inside the triangle. In Fig. 3, we show examples where the vertexes K, P and N, Q converge to the inner vertexes (vertexes inside the triangle) K' and N', respectively.

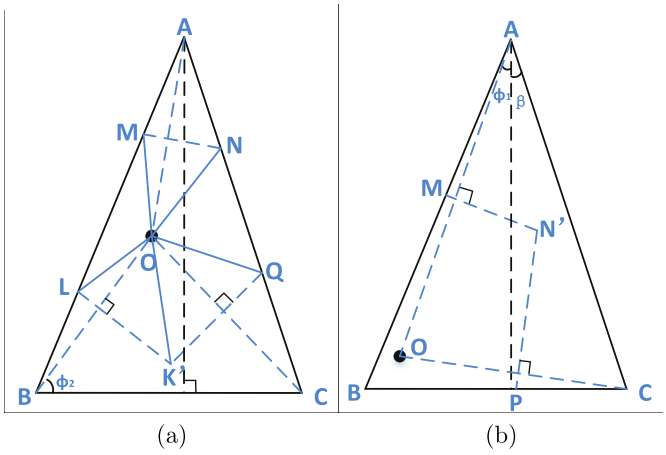

Fig. 3. Examples of K' and N'.

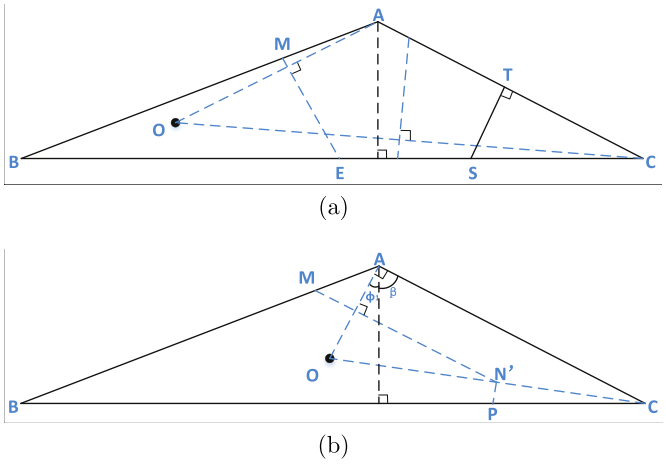

Fig. 4. Example of the disappearance of $\mathbb{V}_3$.

Similarly, M, L may also converge to M'. In total, there are 9 vertexes considered as the candidates of the worst point. We divide them into three vertex sets: $\mathbb{V}^{(1)} = \{M, L, M'\}$, $\mathbb{V}^{(2)} = \{K, P, K'\}$, $\mathbb{V}^{(3)} = \{N, Q, N'\}$. Each set consists of two on-boundary vertexes and one inner vertex. When the inner vertex exists, the on-boundary vertexes in the same set are no longer the valid Voronoi vertexes because it conflicts with the property of Voronoi cells, i.e., the distances from a Voronoi vertex to adjacent service nodes should be the same. Therefore, we have the following Lemma 1.

Lemma 1. *For a vertex set $\mathbb{V}^{(i)}, i = 1, 2, 3$, the Voronoi vertexes can be either the one inner vertex if existed, or the two on-boundary vertexes otherwise.*

Lemma 2. *For $\mathbb{V}^{(1)}$, $\mathbb{V}^{(2)}$, and $\mathbb{V}^{(3)}$, the inner vertexes, i.e., M', K', N', exist only if $\angle AOB \le \frac{\pi}{2}$, $\angle BOC \le \frac{\pi}{2}$, and $\angle AOC \le \frac{\pi}{2}$, respectively.*

Proof. Taking Fig. 3 (a) as an example, given the property of Voronoi cells, K' is the circumcenter of $\triangle BOC$. When $\angle BOC \le \frac{\pi}{2}$, the circumcenter is inside $\triangle BOC$ and thus K' exists. Similar conclusions can be made for M' and N' as well. □

Lemma 3. *In an arbitrary acute triangle, at least one vertex from each vertex sets, i.e., $\mathbb{V}^{(i)}, i = 1, 2, 3$, exist, regardless of the location of the new service node.*

Proof. In some cases, any vertexes from a certain set cannot be found in a triangle. An example is shown in Fig. 4 (a), where N, Q, N' are missing. Two new Voronoi vertexes S and T have been introduced and determined only by the existing service nodes A and C. Furthermore, OA's mid-perpendicular line no longer has the intersection with AC (in the triangle), and a new intersection with BC, vertex E, is introduced.

In Fig. 4 (b), It is observed that N' is the circumcenter of $\triangle AOC$. It will be outside $\triangle AOC$ and below OC only if $\phi_1 + \beta > \frac{\pi}{2}$. Given that $\triangle AOC$ is an acute triangle, $\phi_1 + \beta$ is always smaller than $\frac{\pi}{2}$. Therefore, N' can never move across OC and BC. The situation in Fig. 4 (a) will never happen in an acute triangle. Thus, given OC and OA are in the triangle, N' always exists if $\angle AOC$ is acute, N, Q always exist if $\angle AOC$ is obtuse. Similarly, the existence of vertexes from other sets can be proved in the same way. □

Lemma 4. *In an arbitrary acute triangle, at most one of the inner vertexes, i.e., M', K', or N', exists.*

Proof. According to the proof of Lemma 2, if two vertexes from M', K', and N' exist, two of the angles $\angle AOB$, $\angle BOC$, and $\angle AOC$ are smaller than $\frac{\pi}{2}$. Given $\angle AOB + \angle BOC + \angle AOC = 2\pi$, the rest one angle is larger than π, which means the point O is outside the triangle. All of $\angle AOB$, $\angle BOC$, and $\angle AOC$ cannot be smaller than $\frac{\pi}{2}$ as well. Therefore, at most one vertex from M', K', and N' exists. □

3.2. Problem formulation

In an arbitrary acute triangle formed by three existing service nodes, we want to minimize the service distance of the worst point by optimizing the location of one newly deployed service node. Therefore, the original problem can be transformed to a Min-Max problem of the service distance. Given Lemma 1, 2 and 3 in Sec. 3.1, the optimization problem is given by

$$\min_{O} \quad \max\left(\|OZ_i^{(1)}\|, \|OZ_j^{(2)}\|, \|OZ_k^{(3)}\|\right), \tag{1}$$

$$i = 1, \ldots, \Gamma^{(1)}, j = 1, \ldots, \Gamma^{(2)}, k = 1, \ldots, \Gamma^{(3)},$$

$$\textbf{s.t.} \quad O \in \triangle ABC,$$

$$[Z_1^{(1)}, \ldots, Z_{\Gamma^{(1)}}^{(1)}] = \begin{cases} M', & \angle AOB \le \frac{\pi}{2}, \\ [M, L], & \angle AOB > \frac{\pi}{2}, \end{cases}$$

$$[Z_1^{(2)}, \ldots, Z_{\Gamma^{(2)}}^{(2)}] = \begin{cases} K', & \angle BOC \le \frac{\pi}{2}, \\ [K, P], & \angle BOC > \frac{\pi}{2}, \end{cases}$$

$$[Z_1^{(3)}, \ldots, Z_{\Gamma^{(3)}}^{(3)}] = \begin{cases} N', & \angle AOC \le \frac{\pi}{2}, \\ [N, Q], & \angle AOC > \frac{\pi}{2}, \end{cases}$$

where $\Gamma^{(1)}, \Gamma^{(2)}, \Gamma^{(3)}$ represent the number of currently existing Voronoi vertexes coming from vertex sets $\mathbb{V}^{(1)}, \mathbb{V}^{(2)}, \mathbb{V}^{(3)}$, respectively. For example, when $\triangle AOB \le \frac{\pi}{2}$, there is only one Voronoi vertex M' coming from $\mathbb{V}^{(1)}$, $\Gamma^{(1)} = 1$, and thus $\|OZ_i^{(1)}\|$ denotes only one distance, i.e., $\|OM'\|$. If $\triangle AOB > \frac{\pi}{2}$, there are two Voronoi vertexes, M and L, coming from $\mathbb{V}^{(1)}$, $\Gamma^{(1)} = 2$, and $\|OZ_i^{(1)}\|$ denotes two distances, i.e., $\|OM\|$ and $\|OL\|$.

In the problem formulation, we put $\angle AOB$, $\angle BOC$, and $\angle AOC$ in the condition to study different cases. For example, the objective function is **min** max($\|OM'\|, \|OK\|, \|OP\|, \|ON\|, \|OQ\|$) only if the location of O makes $\angle AOB \le \frac{\pi}{2}$, $\angle BOC > \frac{\pi}{2}$, and $\angle AOC > \frac{\pi}{2}$. The objective function will change to **min** max($\|OM\|, \|OL\|, \|OK'\|, \|ON\|, \|OQ\|$) if the location of O makes $\angle AOB > \frac{\pi}{2}$, $\angle BOC \le \frac{\pi}{2}$, and $\angle AOC > \frac{\pi}{2}$.

Table 1
Global minimizer.

$\alpha \in$	Global minimizer
$[0, 0.106\pi]$	$\|OM\|^*_{\phi_2=A'(\alpha)} = \|OK'\|^*_{\phi_2=A'(\alpha)}$ $= \frac{\|AB\|\cos(\alpha+A'(\alpha))}{2\cos(A'(\alpha))\cos(\alpha)}$;
$[0.106\pi, \frac{\pi}{6}]$	$\|OM\|^*_{\phi_2=A(\alpha)} = \|OK\|^*_{\phi_2=A(\alpha)}$ $= \frac{\|AB\|\cos(\alpha+A(\alpha))}{2\cos(A(\alpha))\cos(\alpha)}$;
$[\frac{\pi}{6}, \frac{\pi}{4}]$	$\|OL\|^*_{\phi_2=\frac{\pi}{4}-\frac{\alpha}{2}} = \|OK\|^*_{\phi_2=\frac{\pi}{4}-\frac{\alpha}{2}}$ $= \frac{\|AB\|\sin(\alpha)}{1+\sin(\alpha)}$;

4. Optimal algorithm design

4.1. Isosceles acute triangle

As a starting point, we assume $\triangle ABC$ is an acute isosceles triangle, i.e. $\|AB\| = \|AC\|$, and thus $\alpha = \beta$.

Lemma 5. *If K' exists in the acute isosceles triangle $\triangle ABC$ where $\|AB\| = \|AC\|$, it is always on BC 's mid-perpendicular line.*

Proof. Given K' is the circumcenter of $\triangle BOC$, $\|K'B\| = \|K'C\|$. Therefore, K' is on BC's mid-perpendicular line. □

Theorem 1. *Given an arbitrary acute isosceles triangle $\triangle ABC$ where $\|AB\| = \|AC\|$, the optimal location of a new service node to minimize the longest service distance is on BC 's mid-perpendicular line.*

Proof. See Appendix A. □

Lemma 6. *Given an acute isosceles triangle $\triangle ABC$ where $\|AB\| = \|AC\|$, if the location of a new service node O is on BC 's mid-perpendicular line and inside $\triangle ABC$, inner vertexes M' and N' do not exist.*

Proof. Given O is on BC's mid-perpendicular line, it is easy to prove $\angle AOB > \frac{\pi}{2}$ and $\angle AOC > \frac{\pi}{2}$. Therefore, the circumcenters of $\triangle AOB$ and $\triangle AOC$ are outside the triangles, and thus there is neither M' nor N' inside $\triangle ABC$. □

Given Theorem 1 and Lemma 6, $\phi_1 = 0$, $\|OM\| = \|ON\|$, $\|OL\| = \|OQ\|$, $\|OK\| = \|OP\|$ and only the inner vertex K' possibly exists in an acute isosceles triangle. We only focus on $\|OM\|$, $\|ON\|$, $\|OK\|$, and $\|OK'\|$ in this section. The service distances to these four candidates of the worst point are derived as follows,

$$\|OM\| = \frac{\|AB\|\cos(\alpha+\phi_2)}{2\cos(\phi_2)\cos(\alpha)}, \tag{2}$$

$$\|OL\| = \frac{\|AB\|\sin(\alpha)}{2\cos(\phi_2)\sin(\alpha+\phi_2)}, \tag{3}$$

$$\|OK\| = \frac{\|AB\|\sin(\alpha)}{2\cos^2(\phi_2)}, \tag{4}$$

$$\|OK'\| = \frac{\|AB\|\sin(\alpha)}{\sin(2\phi_2)}. \tag{5}$$

Theorem 2. *Given an arbitrary acute isosceles triangle, $\triangle ABC$, where $\|AB\| = \|AC\|$ and $\angle OBC = \phi_2$, the optimal location of a new service node (the global minimizer of ϕ_2) and the corresponding minimized service distance to the worst point are summarized in Table 1.*

Proof. See Appendix B. □

It can be observed from Theorem 2 that ϕ_2 is the bisector of $\angle ABC$ when $\alpha \geq \frac{\pi}{6}$. Therefore, given the isosceles triangle, the optimal location is consistent with the incenter of $\triangle ABC$ if $\alpha \geq \frac{\pi}{6}$. For $\alpha < \frac{\pi}{6}$, the optimal location is not any of the existing centers, e.g., incenter, centroid, and circumcenter. Besides, if $\alpha \leq 0.106\pi$, there are 3 worst points with the longest service distance, i.e., M, N, and K'. Otherwise, there are 4 worst points. This observation is generalized by Theorem 3 in the following section.

4.2. Non-isosceles acute triangle

For a non-isosceles acute triangle, we have to consider all of the nine possible vertexes discussed in Sec. 3.1. Given an arbitrary location of O in $\triangle ABC$, i.e., given ϕ_1 and ϕ_2, the service distances to the nine vertexes are derived as follows,

$$\|OM\| = \frac{\|AB\|\cos(\alpha+\phi_2)}{2\cos(\phi_1+\phi_2)\cos(\alpha-\phi_1)}, \tag{6}$$

$$\|ON\| = \frac{\|AC\|\cos(\beta+\phi_3)}{2\cos(\phi_3-\phi_1)\cos(\beta+\phi_1)}, \tag{7}$$

$$\|OL\| = \frac{\|AB\|\sin(\alpha-\phi_1)}{2\cos(\phi_1+\phi_2)\sin(\alpha+\phi_2)}, \tag{8}$$

$$\|OK\| = \frac{\|AB\|\sin(\alpha-\phi_1)}{2\cos(\phi_1+\phi_2)\cos(\phi_2)}, \tag{9}$$

$$\|OP\| = \frac{\|AC\|\sin(\beta+\phi_1)}{2\cos(\phi_1-\phi_3)\cos(\phi_3)}, \tag{10}$$

$$\|OQ\| = \frac{\|AC\|\sin(\beta+\phi_1)}{2\cos(\phi_1-\phi_3)\sin(\beta+\phi_3)}, \tag{11}$$

$$\|OK'\| = \frac{\|AB\|\sin(\alpha+\beta)}{2\sin(\phi_2+\phi_3)\cos(\beta)}, \tag{12}$$

$$\|OM'\| = \frac{\|AB\|}{2\cos(\phi_1+\phi_2)}, \tag{13}$$

$$\|ON'\| = \frac{\|AC\|}{2\cos(\phi_1-\phi_3)}, \tag{14}$$

where

$$\|AC\| = \|AB\|\frac{\cos(\alpha)}{\cos(\beta)},$$

$$\|OA\| = \|AB\|\frac{\cos(\alpha+\phi_2)}{\cos(\phi_1+\phi_2)},$$

and ϕ_3 is $\angle OCB$ and is given by

$$\phi_3 = \arctan\left[\frac{\|AC\|\cos(\beta) - \|OA\|\cos(\phi_1)}{\|OA\|\sin(\phi_1) + \|AC\|\sin(\beta)}\right].$$

Theorem 3. *Given a non-isosceles triangle, $\triangle ABC$, the service distances from the optimal location of a new service node to at least three different Voronoi vertexes are equal to the longest service distance in $\triangle ABC$.*

Proof. See Appendix C. □

Given Theorem 3, we can pick up three different service distances from (6)–(14), make them equal to each other and obtain the result by solving the equation system. A candidate for the longest distance is obtained if the selected distance is the longest compared with other possible distances. After comparing the candidates of all possible combinations, the minimum of the longest distance and the corresponding optimal location (ϕ_1, ϕ_2) can be identified.

According to Lemma 4, at most one service distance from (12)–(14) exists. We propose an equal service distance (ESD) algorithm shown in Algorithm 1 to search the optimal location. The ESD is optimal because all the possible combinations are analyzed.

Algorithm 1 The ESD searching algorithm
Require: $\|AB\|$, α, and β;
1: **for** Every case that chooses three from (6)–(11) **do**
2: Solve the equation system
3: **if** The selected distance is the longest among other possible distances **then**
4: Record the result as a candidate
5: **end if**
6: **end for**
7: **for** Everyone from (12)–(14) **do**
8: Remove the distances to the on-boundary vertexes in the same vertex set defined in Sec. 3.1 from (6)–(11), denote the rest as set $\mathbb{D}$
9: **for** Every case that chooses two from $\mathbb{D}$ **do**
10: Combine with the selected one from (12)–(14)
11: Solve the equation system
12: **if** The selected distance is the longest among other possible distances **then**
13: Record the result as a candidate
14: **end if**
15: **end for**
16: **end for**
17: Compare all the candidates and find out the minimum of the longest service distance and identify the corresponding optimal location
Ensure: the optimal location (ϕ_1, ϕ_2)

Because of the difficulty to derive the closed-form solution of the equation system consisting of three equations from (6)–(14), the numerical method should be adopted, which contributes the major part of the computational load. According to Algorithm 1, we need $\binom{6}{3} = 20$ iterations for on-boundary vertexes and an additional $\binom{4}{2} \times 3 = 18$ iterations to further consider inner vertexes. Overall, 38 equation systems need to be solved to find the optimal location, which greatly reduces the complexity comparing with searching all the points exhaustively inside a triangle.

There are two possible approaches for the supplementary UAV to further obtain the precise optimal location inside the warning area. The first one is to allow the supplementary UAV to communicate with nearby UAVs, and thus it continuously receives the real-time locations of the UAVs forming the warning area. In this way, the supplementary UAV calculates and updates the optimal location, i.e., run the Algorithm 1 by itself. In the second approach, all the UAVs periodically report their GPS coordinates to the control center. The control center runs the Algorithm 1, calculates and updates the optimal location for the supplementary UAV and sends the corresponding GPS coordinate to it. These two approaches are distributed and centralized, respectively. Our proposed algorithm can be realized in either distributed or centralized approaches.

5. Simulation and Verification

To the best of our knowledge, there are no existing solutions to solve the problem formulated in Sec. 3.2. Therefore, in this section, we compare the proposed algorithm with a few benchmarks, such as using the incenter, circumcenter, and centroid as the new service node's locations. The comparisons in term of the maximum service distance are shown to verify the optimality of the proposed solution. Then, we conduct the simulations of a UAV surveillance system to reveal the impacts of the processing time and UAV's speed. We also compare the proposed scheme with the exhaustive search in terms of both the maximum service distance and complexity.

As explained in Sec. 1, the monitoring quality is a function of distance. Given different camera models or other types of monitoring devices like sensors, the functions may vary a lot. Therefore, in this paper, we optimize the distance instead of monitoring quality. As long as the monitoring quality is monotonically decreasing with the increasing of the distance, the longest service distance always represents the worst point. Improving the longest service distance is equivalent to improving the worst monitoring quality which is our objective of this paper. Thus, in Sec. 5, all the performance gains on maximum service distance can directly reflect the gains on monitoring quality.

5.1. Isosceles case

The exhaustive search results have been used to verify the optimal location in an acute isosceles triangle, i.e., Theorem 2. We put BC on the x-axis and let its middle point be the origin point. The height of $\triangle ABC$ is fixed to 100, and we try to find the optimal location given different α. Because the optimal location is always on BC's mid-perpendicular line, which means the x-axis of the optimal location is 0. Thus, we only show the results of the y-axis in Fig. 5. As shown in the figure, the results applying Theorem 2 perfectly match the exhaustive search results.

5.2. Non-isosceles case

For the non-isosceles case, we examine the performance of the proposed scheme in a mobile UAV mesh backbone, i.e., a dynamic triangular warning area. The changing triangle and the trajectory of the optimal location to add the FR are shown in Fig. 6 (a). For comparison, the trajectories of other existing centers of a triangle, including the incenter, circumcenter, and centroid, are shown as well. We start from the equilateral triangle where all the existing centers consistent with the optimal location. With the changing of the triangle, they deviate from each other. We divide the whole time duration of the procedure

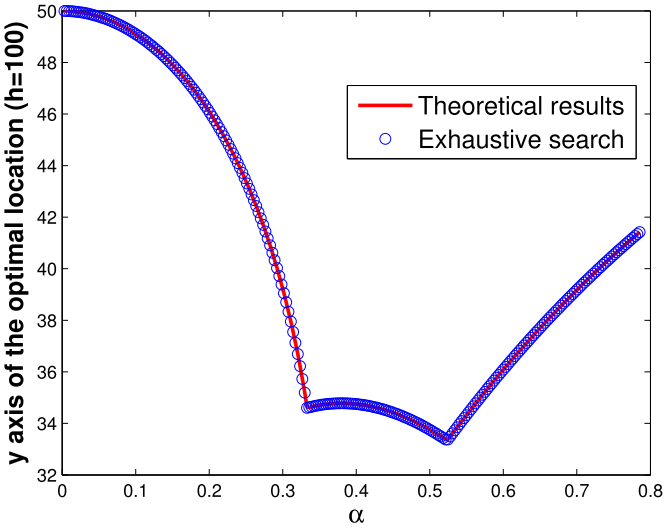

Fig. 5. A triangle formed by three existing service nodes.

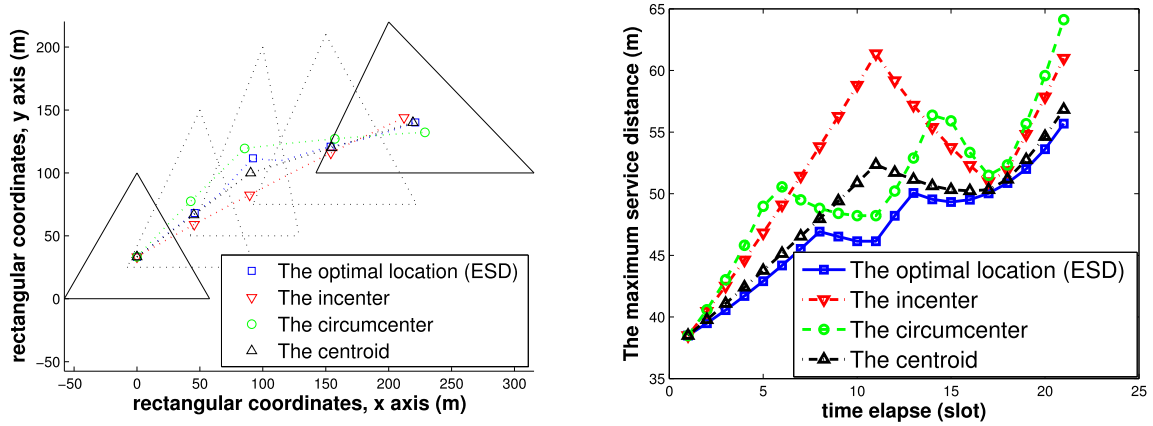

(a) The trace of the optimal location (b) Comparisons with existing centers of a triangle

Fig. 6. Simulation of a dynamic warning area.

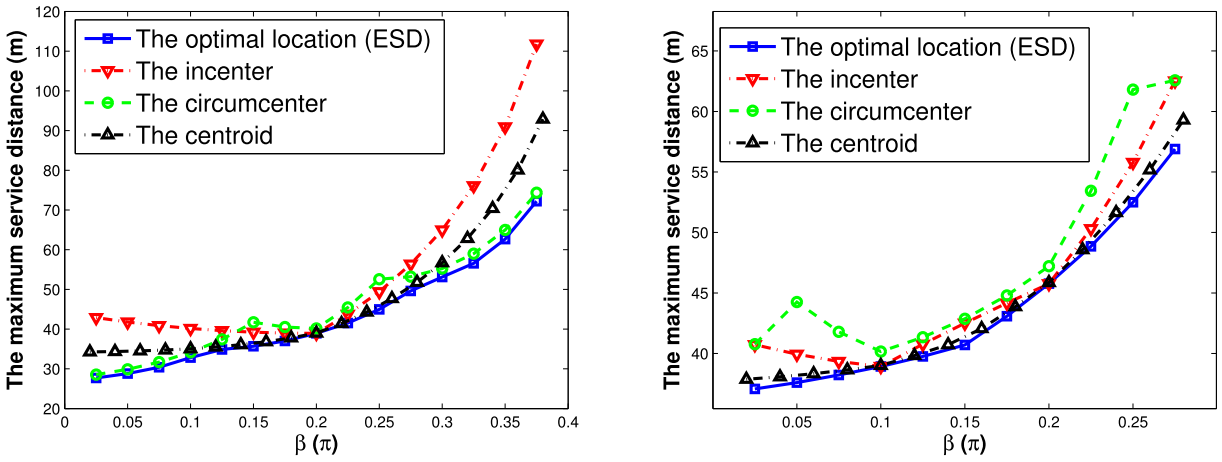

(a) $\alpha = 0.1\pi$ (b) $\alpha = 0.2\pi$

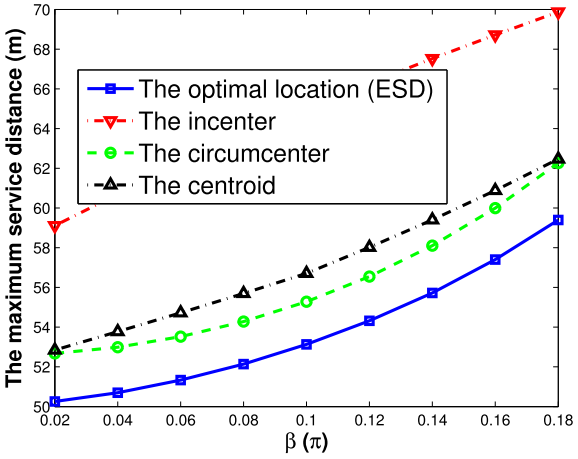

(c) $\alpha = 0.3\pi$

Fig. 7. Comparisons with existing centers of a triangle.

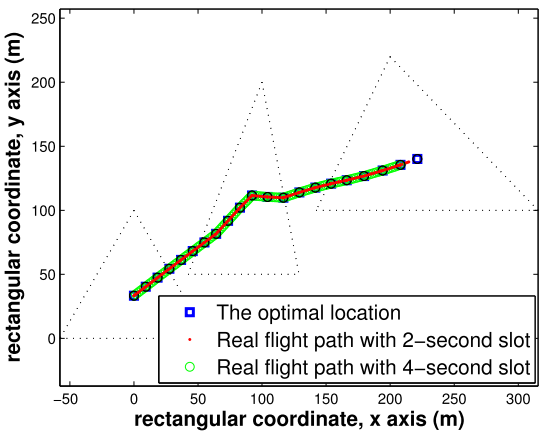

(a) The trace of the real flight path

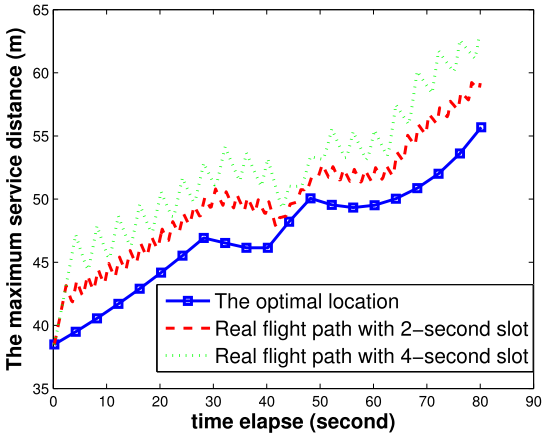

(b) Comparisons between flight paths with different slot length

Fig. 8. Simulation of flight paths given different slot length (t_p = 0.4s).

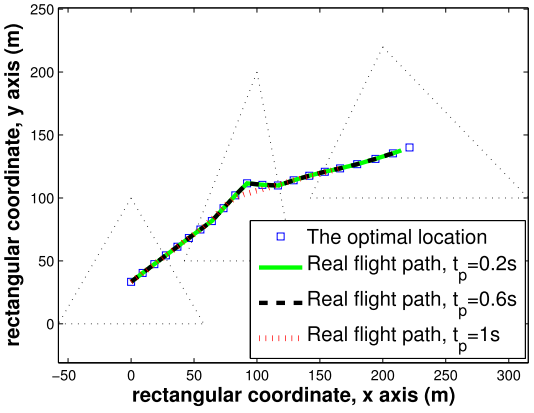

(a) The trace of the real flight path, $v = 5$m/s

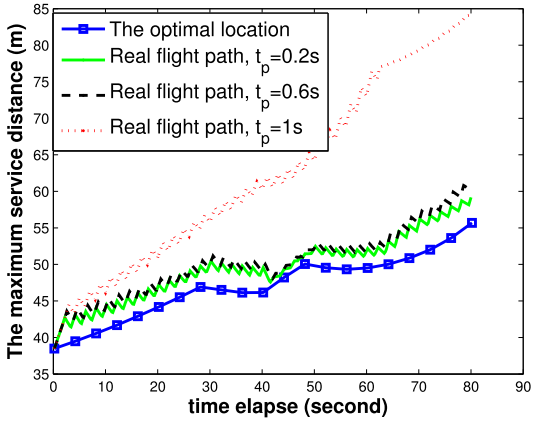

(b) Comparisons between flight paths with different t_p, $v = 5$m/s

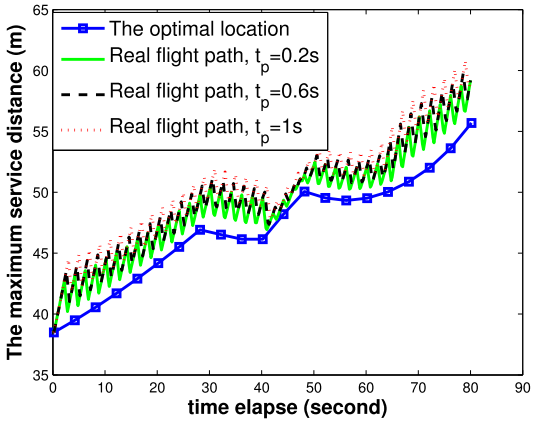

(c) Comparisons between flight paths with different t_p, $v = 10$m/s

Fig. 9. Simulation of flight paths given different t_p (slot length is 2s).

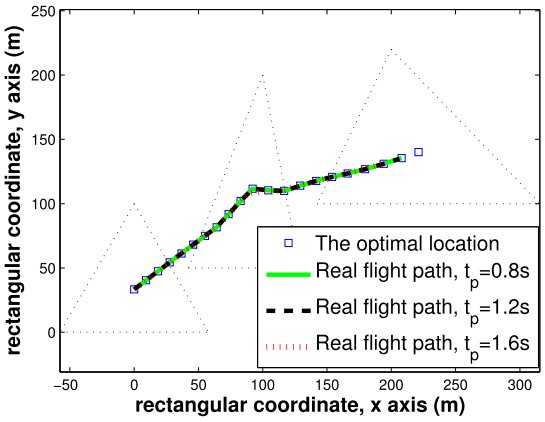

(a) The trace of the real flight path

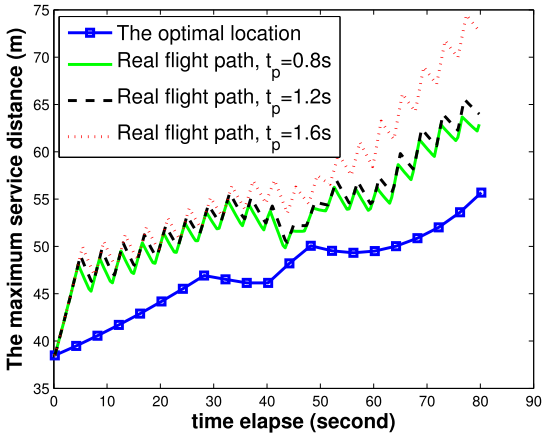

(b) Comparisons between flight paths with different t_p

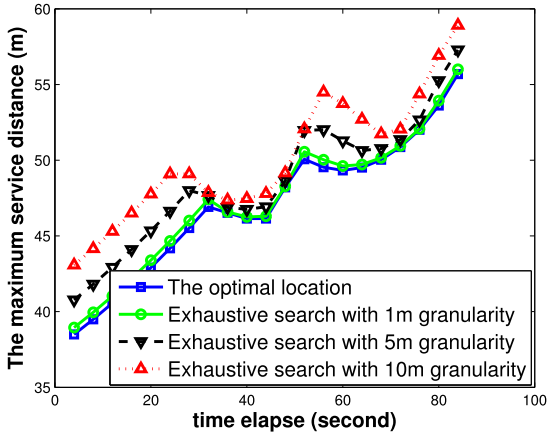

(c) Comparisons with exhaustive search given different searching granularities

Fig. 10. Simulation of flight paths given different t_p (slot length is 4s) and exhaustive search given different searching granularities.

in Fig. 6 (a) into 20 equal slots, and record the maximum service distance of each slot in Fig. 6 (b). It can be observed that the proposed scheme can always achieve a better performance than other existing centers. On average, it can reduce the maximum service distance by 9.52%, 6.79%, and 2.86% compared to the incenter, circumcenter, and centroid, respectively.

In order to have a more comprehensive investigation, we compare the maximum service distance achieved by the proposed approach with that of other existing centers exhaustively. α and β are adjusted to cover all the possible cases. The height of $\triangle ABC$, i.e., BC's perpendicular line passing through service node A, is fixed to 100 m. The maximum service distances according to different locations of the newly added service node are summarized in Fig. 7 α is equal to 0.1π, 0.2π, and 0.3π in Fig. 7 (a), (b), and (c), respectively. It can be observed that the maximum service distance achieved by the proposed scheme is always the lower-bound, and thus verifies the optimality. The proposed ESD algorithm can reduce the maximum service distance by up to 35.71%, 15.91%, and 21.74% compared to the incenter, circumcenter, and centroid, respectively.

5.3. Performance evaluation regarding to UAV's flight path

In this subsection, we examine the maximum service distance along the UAV's flight path. The results based on different slot duration, i.e., how long the UAV updates its location, are shown in Fig. 8. We apply the same changing mesh backbone in Fig. 6 (a) and assume the procedure lasts for 80 s. The maximum actual speeds of three existing service nodes, i.e., three vertexes of the changing triangle, are 3.54 m/s, 2.80 m/s, and 4.83 m/s, respectively. A maximum speed limit of 5 m/s is assumed for the newly added UAV which always updates the location based on the latest information of the mesh.

The flight paths with 2-s and 4-s slot durations are almost the same with the trace strung by optimal locations, as shown in Fig. 8 (a). The maximum service distances along their flight paths are quite different as shown in Fig. 8 (b). Compared with 4-s slot, 2-s slot reduces the average gap to the optimal result from 6.15 m to 3.03 m. It is because a smaller slot duration results in a smaller deviation to the optimal location before the UAV's next update.

However, the slot duration is not always the smaller the better. The processing time t_p, i.e., the time needed by a UAV to calculate the updated location, also plays an important role. We use $t_p = 0.4$s in Fig. 8 and the effects of different t_p are revealed in Fig. 9. A smaller t_p means a longer time for moving, and thus the UAV has a higher chance to reach the newly updated location. Given a fixed t_p, a small slot duration means a shorter moving time, the UAV may be unable to catch up the speed of the optimal location, e.g., $t_p = 1$s in Fig. 9 (a) and (b).

Given $t_p = 1$s, one way to improve the performance is to increase the UAV's speed. In Fig. 9 (c) it shows that the UAV keeps pace with the updated location well if the speed is increased to $v = 10$ m/s. Considering mechanical issues, however, it may be difficult to further enhance the speed given the cost of a UAV. So, the slot duration needs to be prolonged to reduce the proportion of processing time. In Fig. 10 (a) and (b), the system can support up to $t_p = 1.2$s if the slot length is 4s. But the average gap of the maximum service distance to the optimal result is enlarged to 6.49 m. This observation justifies the necessity of the proposed low-complexity ESD algorithm, by which a smaller slot duration can be used to achieve better performance.

Exhaustive search results with different granularities are shown in Fig. 10 (c). A coarser granularity reduces the complexity but significantly increases the gap between the updated locations and the optimal ones. Otherwise, it results in a large t_p and is not suitable for real-time updating especially when the size of the warning area, i.e., the triangle, is large. For example, in Fig. 10 (c), when we choose a 1-m granularity for the exhaustive search, 5000–10,000 points needs to be searched in each slot according to the dynamic shape of the triangle. In practice, if a finer granularity and/or a bigger triangle area are used, the number can be even larger. Comparing with the heavy workload of the exhaustive search, only 38 equation systems need to be solved to find the optimal location in the proposed ESD algorithm as analyzed in Sec. 4.2, which will greatly reduce t_p and thus provide a better performance as shown in Fig. 9 (b), (c), and Fig. 10 (b).

6. Conclusion

For the UAV surveillance system, we have proposed a second stage in addition to the existing seamless surveillance (the first stage), where a supplementary UAV is introduced to provide high-quality monitoring in the warning area. A min-max optimization problem has been formulated to minimize the longest service distance in an arbitrary acute triangle. For the newly added service node, the closed-form expression of the optimal location within an isosceles triangle has been theoretically derived. An ESD algorithm with low complexity has been proposed to find the optimal location of the new service node within a non-isosceles triangle as well. The numerical comparisons with the exhaustive search results and triangle's existing centers, including incenter, circumcenter, and centroid, have been conducted, according to which the optimality of the proposed approach has been validated. The impacts of UAV's speed and processing time on the performance have been studied.

This work can be applied to other areas. In summary, when a new facility needs to be added to improve the experience of the worst user, this work is applicable. The worst user is the customer with the lowest quality of service (QoS), which can be the slowest response time in police, ambulance, or fire services, the longest travel distance to a supermarket, a postal office, or a recreation center, or the lowest signal strength in the wireless communication system such as cellular and Wi-Fi networks. Though it is not the surveillance system, the worst possible experience is also important for a service provider because it determines the guaranteed QoS advertised. For example, in the cellular system, the cell edge user throughput, which is defined as the 5% point of cumulative distribution function (CDF) of the user throughput normalized with the overall cell bandwidth, has been applied as a critical performance metric to evaluate the system (3GPP, 2017).

Some possible future works have been identified. In this paper, we focus on the acute triangle, which may impose restrictions on UAVs' deployment for the first-stage coverage, i.e., ensuring all the warning areas are acute triangles. Obtuse triangles can be studied and thus provide higher flexibility. The homogeneous service node has been assumed in this paper which means all the service node have the same capability and the monitoring/service quality only depends on the service distance. Heterogeneous service nodes and differentiated areas, i.e., areas with different weights, are worth for research. Based on a newly defined optimizing objective combining the service node's capability, the area weight, and the service distance, the solution will be applicable to more scenarios. Besides, only one new service node in a 2-D plane has been considered in this paper. How to coordinate multiple supplementary service nodes in 3-D space for the same purpose beckons for further investigation. In the 3-D case, no matter how the UAVs change their altitudes, the triangular warning area forms one plane. It is always possible to project targets and supplementary UAV on that plane and remodel the service distances accordingly. This projection requires careful future research.

In addition to the theoretical research, the implementation aspects need to be considered as well. This paper is based on the assumption that the UAV can move to the designated location once it obtains the command (received from the control center or calculated by itself). How to adjust aerodynamic power to achieve this target and how to avoid possible obstacles are still open issues. The mature platform like Microsoft AirSim can be used to evaluate the performance before the prototype phase.

Conflicts of interest

None.

Acknowledgments

This work was supported in part by the Natural Sciences and Engineering Research Council of Canada (NSERC), the Canada Foundation for Innovation (CFI)/BC Knowledge Development Fund (BCKDF), the Compute Canada, the China Scholarship Council (CSC), and the National Natural Science Foundation of China (NSFC) under Grant 61702450.

Appendix A. Proof of Theorem 1

As shown in Fig. A.11 (a), we assume a point O_1 in the left side of BC's mid-perpendicular line, and five vertexes are marked as M_1, L_1, K'_1, Q_1, and N_1. If O_1 moves horizontally to O_0, which is on BC's mid-perpendicular line, the vertexes change to M_1, L_1, K'_1, Q_1, and N_1. We consider K' in this figure, and the case of K and P is shown in Fig. A.11 (b).

Given the property of Voronoi cells, M_1N_1, M_0N_0, and AO_1 intersect at the same point, It is easy to get $\|AM_1\| < \|AN_1\|$, $\|AM_1\| < \|AM_0\|$, and $\|AN_1\| > \|AN_0\|$. Because $\|M_1O_1\| = \|AM_1\|$, $\|N_1O_1\| = \|AN_1\|$, $\|M_0O_0\| = \|AM_0\|$, $\|N_0O_0\| = \|AN_0\|$, we have $\|M_1O_1\| < \|N_1O_1\|$, $\|M_1O_1\| < \|M_0O_0\|$, and $\|N_1O_1\| > \|N_0O_0\|$. Therefore, we can conclude that once point O locates in the left side of BC's mid-perpendicular line, $\|ON\|$ is always longer than $\|OM\|$, and when O moves horizontally toward the mid-perpendicular line, the difference between $\|ON\|$ and $\|OM\|$ is reduced.

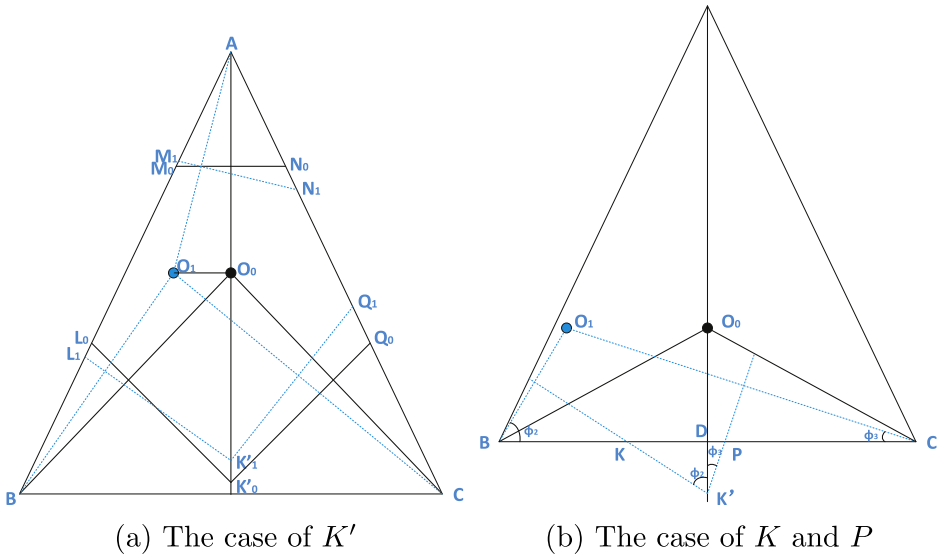

(a) The case of K' (b) The case of K and P

Fig. A 11 Changes of the vertexes when O moves horizontally.

$\|LK\|$ and $\|QP\|$ will intersect at K' which locates on the mid-perpendicular line or its extension line (outside $\triangle ABC$). Given the topology in Fig. A.11 (a), $\angle L_1K'_1O_0 > \angle Q_1K'_1O_0$. Thus $\|BL_1\| < \|CQ_1\|$ and $\|O_1L_1\| < \|O_1Q_1\|$. If O_1 moves to O_0, it is easy to prove $\|BL_1\| < \|BL_0\|$ and $\|CQ_1\| > \|CQ_0\|$, so that $\|O_1L_1\| < \|O_0L_0\|$ and $\|O_1Q_1\| > \|O_0Q_0\|$. Therefore, when O is in the left side of BC's mid-perpendicular line, $\|OQ\|$ is always longer than $\|OL\|$, and the difference decreases while O moving from O_1 to O_0.

We use Fig. A.11 (b) to discuss the case of K and P. It is easy to find out $\|OK\| = \frac{\|BC\|}{2} - \|DK\|$, $\|OP\| = \frac{\|BC\|}{2} - \|DP\|$, $\angle KK'D = \phi_2$, and $\angle PK'D = \phi_3$. Given that O is in the left side of BC's mid-perpendicular line, such as O_1 in the figure, $\phi_2 > \phi_3$. Thus, $\|KD\| > \|DP\|$, and $\|OK\| < \|OP\|$. If O moves horizontally from O_1 to O_0, ϕ_2 gets close to ϕ_3, so do $\|OK\|$ and $\|OP\|$.

For the case of K' shown in Fig. A.11 (a), K' is always the circumcenter of $\triangle OBC$. Given Lemma 5, if O moves from O_0 to O_1, vertex K' shall move upward from K'_0 to K'_1, in order to satisfy $\|K'B\| = \|K'C\| = \|OK'\|$. Therefore, $\|O_1K'_1\| > \|O_0K'_0\|$. We can conclude that when O moves horizontally toward the mid-perpendicular line, $\|OK'\|$ is decreasing. A similar approach can be applied to prove that $\|ON'\|$ holds the same conclusion. (There is no M' inside the triangle when O is in the left side because $\angle AOB > \frac{\pi}{2}$.)

In summary, when there is no vertex in M', K', and N' exists and O is in the left side of BC's mid-perpendicular line, $\max(\|OM\|, \|OL\|, \|OK\|) < \max(\|ON\|, \|OQ\|, \|OP\|)$. The longest service distance is one of $\|ON\|$, $\|OQ\|$, $\|OP\|$, and it is decreasing while O moving toward the mid-perpendicular line. If inner vertex exists (according to Lemma 4 at most one of them exists), such as K' or N', the corresponding service distance is also decreasing while O moving toward the mid-perpendicular line. It is easy to proof the same conclusions if O is in the right side of the mid-perpendicular line. It can be concluded that the maximum service distance is decreasing while the location of a new service node O moving horizontally toward the mid-perpendicular line. Therefore, the optimal location of a new service node is on BC's mid-perpendicular line.

Appendix B. Proof of Theorem 2

When $\|OK'\| \leq \|OK\|$, K' will be used instead of K as a valid Voronoi vertex in the triangle.

$$\|OK'\| \leq \|OK\|$$

$$\Longrightarrow \frac{\|AB\|\sin(\alpha)}{\sin(2\phi_2)} \leq \frac{\|AB\|\sin(\alpha)}{2\cos(\phi_2)^2}$$

$$\Longrightarrow \sin(\phi_2) \geq \cos(\phi_2). \tag{B.1}$$

Given (B.1), when $0 \leq \phi_2 \leq \frac{\pi}{4}$, $\|OK\|$ is used in the following analysis. When $\frac{\pi}{4} \leq \phi_2 \leq \frac{\pi}{2}$, $\|OK'\|$ will be applied. $\|OK'\| = \|OK\|$ when. $\phi_2 = \frac{\pi}{4}$

Appendix B.1. If $\|OL\|$ is the maximum distance

Assuming that $\|OL\|$ is the longest transmission distance, we have

$$\|OL\| \geq \|OK'\|$$
$$\Longrightarrow \sin(\phi_2) \geq \sin(\alpha + \phi_2). \tag{B.2}$$

Given $\phi_2 \leq \frac{\pi}{2}, \alpha + \phi_2 \leq \frac{\pi}{2}$, the inequality above is impossible, which means $\|OL\|$ cannot be larger than $\|OK'\|$. Therefore, $\|OK'\|$ does not exist when $\|OL\|$ is the longest distance.

When $0 \leq \phi_2 \leq \frac{\pi}{4}$, $\|OK\|$ is used and we have

$$\|OL\| \geq \|OK\|$$
$$\Longrightarrow \sin(\alpha + \phi_2) \leq \cos(\phi_2)$$
$$\Longrightarrow \phi_2 \in \left[0, \frac{\pi}{4} - \frac{\alpha}{2}\right]. \tag{B.3}$$

$$\|OL\| \geq \|OM\|$$
$$\Longrightarrow \sin(2\alpha) \geq \sin(2\alpha + 2\phi_2)$$
$$\Longrightarrow \phi_2 \in \left[\max\{\frac{\pi}{2} - 2\alpha, 0\}, \frac{\pi}{2} - \alpha\right]. \tag{B.4}$$

Taking the intersection of the two sets above and considering the fact that $0 \leq \phi_2 \leq \frac{\pi}{4}$ and $0 \leq \alpha \leq \frac{\pi}{4}$, we have

$$\phi_2 \in \left[0, \frac{\pi}{4} - \frac{\alpha}{2}\right] \bigcap \left[\max\{\frac{\pi}{2} - 2\alpha, 0\}, \frac{\pi}{2} - \alpha\right]$$
$$= \begin{cases} \emptyset, & \alpha \in \left[0, \frac{\pi}{6}\right), \\ \left[\frac{\pi}{2} - 2\alpha, \frac{\pi}{4} - \frac{\alpha}{2}\right], & \alpha \in \left[\frac{\pi}{6}, \frac{\pi}{4}\right]. \end{cases} \tag{B.5}$$

We calculate the derivative of $\|OL\|$ w.r.t. ϕ_2 as follows,

$$\frac{\partial \|OL\|}{\partial \phi_2} = \frac{\|AB\| \sin(\alpha)}{2} \times \frac{\sin(\phi_2)\sin(\alpha + \phi_2) - \cos(\phi_2)\cos(\alpha + \phi_2)}{\left[\cos(\phi_2)\sin(\alpha + \phi_2)\right]^2}$$
$$= -\frac{\|AB\| \sin(\alpha)\cos(2\phi_2 + \alpha)}{2\left[\cos(\phi_2)\sin(\alpha + \phi_2)\right]^2}, \tag{B.6}$$

where only $\cos(2\phi_2 + \alpha)$ needs to be discussed, and other items are obviously positive. Let $\cos(2\phi_2 + \alpha) = 0$, we can obtain that $\phi_2 = \frac{\pi}{4} - \frac{\alpha}{2}$, which is the upper bound of ϕ_2 in (B.5) given that $\|OL\|$ is the longest distance ($\alpha \geq \frac{\pi}{6}$). Considering $\frac{\partial \|OL\|}{\partial \phi_2} \leq 0$ when $\phi_2 \leq \frac{\pi}{4} - \frac{\alpha}{2}$, and $\frac{\partial \|OL\|}{\partial \phi_2} \geq 0$ when $\phi_2 \geq \frac{\pi}{4} - \frac{\alpha}{2}$, $\phi_2 = \frac{\pi}{4} - \frac{\alpha}{2}$ is the minimizer of $\|OL\|$.

Therefore, we can conclude that if $\|OL\|$ is the longest distance ($\alpha \geq \frac{\pi}{6}$), the minimum of $\|OL\|$ can be obtained as follows,

$$\|OL\|^* = \|OL\|_{\phi_2 = \frac{\pi}{4} - \frac{\alpha}{2}}$$
$$= \frac{\|AB\| \sin(\alpha)}{2\cos(\frac{\pi}{4} - \frac{\alpha}{2})\sin(\frac{\pi}{4} + \frac{\alpha}{2})}$$
$$= \frac{\|AB\| \sin(\alpha)}{1 + \sin(\alpha)}. \tag{B.7}$$

Appendix B.2. If $\|OM\|$ is the maximum distance

Assuming that $\|OM\|$ is the longest transmission distance, we first compare it with $\|OK\|$ and $\|OL\|$, respectively.

$$\|OM\| \geq \|OK\|$$
$$\Longrightarrow \frac{\cos(\alpha + \phi_2)}{\cos(\alpha)} \geq \frac{\sin(\alpha)}{\cos(\phi_2)}$$
$$\Longrightarrow \cos(\alpha + 2\phi_2) + \cos(\alpha) \geq \sin(2\alpha). \tag{B.8}$$

Because of $0 \leq \alpha + 2\phi_2 \leq \pi$ and the fact that cosine function is monotonically decreasing in this range, we can obtain the following range of ϕ_2 to satisfy (B.8).

$$\phi_2 \leq \frac{\arccos\left[\sin(2\alpha) - \cos(\alpha)\right] - \alpha}{2} = A(\alpha) \tag{B.9}$$

Similarly,

$$\|OM\| \geq \|OL\|$$

$$\Longrightarrow \frac{\cos(\alpha+\phi_2)}{\cos(\alpha)} \geq \frac{\sin(\alpha)}{\sin(\alpha+\phi_2)}$$

$$\Longrightarrow \sin(2\alpha+2\phi_2) \geq \sin(2\alpha)$$

$$\Longrightarrow \phi_2 \in \left[0, \max\left(\frac{\pi}{2}-2\alpha, 0\right)\right]. \tag{B.10}$$

From (B.10), it can be observed that if $\alpha \geq \frac{\pi}{4}$ (obtuse triangle), $\|OM\|$ cannot be the longest distance.

It is easy to find out that $A(\alpha) \leq \frac{\pi}{2}-2\alpha$ when $\alpha \in [0, \frac{\pi}{6}]$, and $A(\alpha) \geq \frac{\pi}{2}-2\alpha$ when $\alpha \in [\frac{\pi}{6}, \frac{\pi}{4}]$. Taking the intersection of two ranges derived in (B.10) and (B.9), we have

$$\phi_2 \in \left[0, A(\alpha)\right] \bigcap \left[0, \max\{\frac{\pi}{2}-2\alpha, 0\}\right]$$

$$= \begin{cases} \left[0, A(\alpha)\right], & \alpha \in \left[0, \frac{\pi}{6}\right], \\ \left[0, \frac{\pi}{2}-2\alpha\right], & \alpha \in \left[\frac{\pi}{6}, \frac{\pi}{4}\right]. \end{cases} \tag{B.11}$$

The derivative of $\|OM\|$ w.r.t. ϕ_2 is given as follows,

$$\frac{\partial\|OM\|}{\partial\phi_2} = \frac{\|AB\|}{2\cos(\alpha)} \times \frac{-\sin(\alpha+\phi_2)\cos(\phi_2)+\cos(\alpha+\phi_2)\sin(\phi_2)}{\left[\cos(\phi_2)\right]^2}$$

$$= -\frac{\|AB\|\sin(\alpha)}{2\cos(\alpha)\left[\cos(\phi_2)\right]^2}, \tag{B.12}$$

It can be observed that given $\alpha \leq \frac{\pi}{2}$, $\frac{\partial\|OM\|}{\partial\phi_2} \leq 0$, so that the upper bound of ϕ_2 is a minimizer of $\|OM\|$. It should be noticed that $\|OK\|$ is considered only if $0 \leq \phi_2 \leq \frac{\pi}{4}$, otherwise, $\|OK'\|$ will be applied.

Therefore, if $\|OM\|$ is the longest distance, the minimum of $\|OM\|$ is given by

$$\|OM\|^* = \|OM\|_{\phi_2=A(\alpha)}$$

$$= \frac{\|AB\|\cos(\alpha+A(\alpha))}{2\cos(A(\alpha))\cos(\alpha)}, \tag{B.13}$$

when

$$\left[A(\alpha) \leq \frac{\pi}{4}\right] \bigcap \left[\alpha \leq \frac{\pi}{6}\right]$$

$$= \left[\arccos\left[\sin(2\alpha)-\cos(\alpha)\right] \leq \frac{\pi}{2}+\alpha\right] \bigcap \left[\alpha \leq \frac{\pi}{6}\right]$$

$$= \left[\sin(2\alpha)-\cos(\alpha)+\sin(\alpha) \geq 0\right] \bigcap \left[\alpha \leq \frac{\pi}{6}\right]$$

$$\Longrightarrow \alpha \in \left[0.106\pi, \frac{\pi}{6}\right], \tag{B.14}$$

and

$$\|OM\|^* = \|OM\|_{\phi_2=\frac{\pi}{2}-2\alpha}$$

$$= \frac{\|AB\|\sin(\alpha)}{2\sin(2\alpha)\cos(\alpha)}$$

$$= \frac{\|AB\|}{4\cos^2(\alpha)}. \tag{B.15}$$

when

$$\left[\frac{\pi}{2}-2\alpha \leq \frac{\pi}{4}\right] \bigcap \left[\frac{\pi}{6} \leq \alpha \leq \frac{\pi}{4}\right]$$

$$\Longrightarrow \alpha \in \left[\frac{\pi}{6}, \frac{\pi}{4}\right]. \tag{B.16}$$

If $\|OK'\|$, instead of $\|OK\|$, is applied, we have

$$\|OM\| \geq \|OK'\|$$

$$\Longrightarrow \frac{\cos(\alpha+\phi_2)}{\cos(\alpha)} \geq \frac{\sin(\alpha)}{\sin(\phi_2)}$$

$$\Longrightarrow \sin(\alpha+2\phi_2) \geq \sin(2\alpha)+\sin(\alpha). \tag{B.17}$$

When $\|OK'\|$ is applied, $\phi_2 \geq \frac{\pi}{4}$. Thus, $\frac{\pi}{2} \leq \alpha+2\phi_2 \leq \pi$, and the sine function is monotonically decreasing in this range. Therefore, we have

$$\phi_2 \leq \frac{\pi-\arcsin\left[\sin(2\alpha)+\sin(\alpha)\right]-\alpha}{2} = A'(\alpha) \tag{B.18}$$

Also, we can observe that if $\sin(2\alpha) + \sin(\alpha) \geq 1$, (B.18) does not hold, and thus $\|OM\|$ is not the longest distance. The valid range can be calculated as follows,

$$\begin{aligned} &\sin(2\alpha) + \sin(\alpha) \leq 1 \\ \Longrightarrow &2\sin(\alpha)\sqrt{1-\sin^2(\alpha)} + \sin(\alpha) \leq 1 \end{aligned} \tag{B.19}$$

Let $x = \sin(\alpha)$, it can be rewritten as

$$\begin{aligned} &4x^4 - 3x^2 - 2x + 1 \geq 0 \\ \Longrightarrow &(x-1)(4x^3 + 4x^2 + x - 1) \geq 0 \end{aligned} \tag{B.20}$$

Because of $\phi_2 \geq \frac{\pi}{4}$, $\alpha \leq \frac{\pi}{4}$ and thus $x - 1 = \sin(\alpha) - 1 \leq 0$,

$$\Longrightarrow (4x^3 + 4x^2 + x - 1) \leq 0 \tag{B.21}$$

Based on the numerical calculation, we find that (B.21) holds when $x \leq 0.348$. Therefore, (B.18) holds when $\alpha \leq \arcsin(0.348)$. It is easy to find that when $\alpha \leq \arcsin(0.348)$, $\max(\frac{\pi}{2} - 2\alpha, 0)$ is always larger than $A'(\alpha)$. The intersection of the ranges in (B.18) and (B.11), i.e., the condition of $\|OM\| \geq \|OL\|$, is given by

$$\begin{aligned} \phi_2 &\in \left[0, A'(\alpha)\right] \bigcap \left[0, \max\left(\frac{\pi}{2} - 2\alpha, 0\right)\right] \\ &= \left[0, A'(\alpha)\right], \alpha \in [0, \arcsin(0.348)]. \end{aligned} \tag{B.22}$$

It has been shown in (B.12) that $\|OM\|$ is monotonically decreasing with the increasing of ϕ_2. Therefore, $\phi_2 = A'(\alpha)$ is a minimizer of $\|OM\|$. In order to satisfy the existence of $\|OK'\|$, we have

$$\begin{aligned} &A'(\alpha) \geq \frac{\pi}{4} \\ \Longrightarrow &\cos(\alpha) - \sin(2\alpha) - \sin(\alpha) \geq 0 \\ \Longrightarrow &\alpha \leq 0.106\pi. \end{aligned} \tag{B.23}$$

It is easy to find that $[0, 0.106\pi] \cap [0, \arcsin(0.348)] = [0, 0.106\pi]$, so we have

$$\begin{aligned} \|OM\|^* &= \|OM\|_{\phi_2 = A'(\alpha)} \\ &= \frac{\|AB\|\cos(\alpha + A'(\alpha))}{2\cos(A'(\alpha))\cos(\alpha)}, \quad \alpha \in [0, 0.106\pi]. \end{aligned} \tag{B.24}$$

Appendix B.3. If $\|OK\|$ is the maximum distance

First, let $\phi_2 \leq \frac{\pi}{4}$ to ensure the existence of $\|OK\|$. Similar to the results we obtained from Sec. Appendix B.1 & Appendix B.2, we have

$$\begin{aligned} &\|OL\| \leq \|OK\| \\ \Longrightarrow &\sin(\alpha + \phi_2) \geq \cos(\phi_2) \\ \Longrightarrow &\phi_2 \in \left[\frac{\pi}{4} - \frac{\alpha}{2}, \frac{\pi}{4}\right], \end{aligned} \tag{B.25}$$

and

$$\begin{aligned} &\|OM\| \leq \|OK\| \\ \Longrightarrow &\cos(\alpha + 2\phi_2) + \cos(\alpha) \leq \sin(2\alpha) \\ \Longrightarrow &\phi_2 \in \left[A(\alpha), \frac{\pi}{4}\right]. \end{aligned} \tag{B.26}$$

If $A(\alpha) > \frac{\pi}{4} \Longrightarrow \alpha < 0.106\pi$, there is no feasible solution. Considering $\alpha \geq 0.106\pi$, the valid range of ϕ_2 is given by

$$\begin{aligned} \phi_2 &\in \left[\frac{\pi}{4} - \frac{\alpha}{2}, \frac{\pi}{4}\right] \bigcap \left[A(\alpha), \frac{\pi}{4}\right] \\ &= \begin{cases} \left[\frac{\pi}{4} - \frac{\alpha}{2}, \frac{\pi}{4}\right], & \alpha \in \left[\frac{\pi}{6}, \frac{\pi}{2}\right], \\ \left[A(\alpha), \frac{\pi}{4}\right], & \alpha \in \left[0.106\pi, \frac{\pi}{6}\right]. \end{cases} \end{aligned} \tag{B.27}$$

The derivative of $\|OK\|$ w.r.t. ϕ_2 can be obtained as follows,

$$\begin{aligned} \frac{\partial\|OK\|}{\partial\phi_2} &= \frac{\|AB\|\sin(\alpha)}{2} \frac{2\cos(\phi_2)\sin(\phi_2)}{\left[\cos(\phi_2)\right]^4} \\ &= \frac{\|AB\|\sin(\alpha)\sin(\phi_2)}{\left[\cos(\phi_2)\right]^3} \geq 0. \end{aligned} \tag{B.28}$$

Therefore, when $\|OK\|$ is the longest distance, the minimum of $\|OK\|$ is given by

$$\|OK\|^* = \|OK\|_{\phi_2=A(\alpha)} = \frac{\|AB\|\sin(\alpha)}{2\cos^2(A(\alpha))}, \quad \alpha \in \left[0.106\pi, \frac{\pi}{6}\right]. \tag{B.29}$$

and

$$\|OK\|^* = \|OK\|_{\phi_2=\frac{\pi}{4}-\frac{\alpha}{2}} = \frac{\|AB\|\sin(\alpha)}{1+\sin(\alpha)}, \quad \alpha \in \left[\frac{\pi}{6}, \frac{\pi}{2}\right]. \tag{B.30}$$

Appendix B.4. If $\|OK'\|$ is the maximum distance

If $\|OK'\|$ is applied, $\phi_2 \geq \frac{\pi}{4}$ and $\alpha \leq \frac{\pi}{4}$. Similarly, we have

$$\|OL\| \leq \|OK'\| \Longrightarrow \sin(\phi_2) \leq \sin(\alpha+\phi_2). \tag{B.31}$$

and

$$\|OM\| \leq \|OK'\| \Longrightarrow \phi_2 \geq \frac{\pi - \arcsin\left[\sin(2\alpha)+\sin(\alpha)\right] - \alpha}{2} = A'(\alpha) \tag{B.32}$$

It is obvious that (B.31) is always true given $\alpha + \phi_2 \leq \frac{\pi}{2}$. So the valid range of ϕ_2 is given by

$$\phi_2 \in \begin{cases} \left[\frac{\pi}{4}, \frac{\pi}{2}\right], & \alpha \in \left[0.106\pi, \frac{\pi}{4}\right], \\ \left[A'(\alpha), \frac{\pi}{2}\right], & \alpha \in [0, 0.106\pi]. \end{cases} \tag{B.33}$$

Table B.2
Candidate minimizers

$\alpha \in$	Candidate minimizers and the longest distances
$[0, 0.106\pi]$	$\|OM\|^*_{\phi_2=A'(\alpha)} = \frac{\|AB\|\cos(\alpha+A'(\alpha))}{2\cos(A'(\alpha))\cos(\alpha)}$,
	$\|OK'\|^*_{\phi_2=A'(\alpha)} = \frac{\|AB\|\sin(\alpha)}{\sin(2A'(\alpha))}$;
$[0.106\pi, \frac{\pi}{6}]$	$\|OM\|^*_{\phi_2=A(\alpha)} = \frac{\|AB\|\cos(\alpha+A(\alpha))}{2\cos(A(\alpha))\cos(\alpha)}$,
	$\|OK\|^*_{\phi_2=A(\alpha)} = \frac{\|AB\|\sin(\alpha)}{2\cos^2(A(\alpha))}$,
	$\|OK'\|^*_{\phi_2=\frac{\pi}{4}} = \|AB\|\sin(\alpha)$;
$[\frac{\pi}{6}, \frac{\pi}{4}]$	$\|OL\|^*_{\phi_2=\frac{\pi}{4}-\frac{\alpha}{2}} = \frac{\|AB\|\sin(\alpha)}{1+\sin(\alpha)}$,
	$\|OM\|^*_{\phi_2=\frac{\pi}{2}-2\alpha} = \frac{\|AB\|}{4\cos^2(\alpha)}$,
	$\|OK\|^*_{\phi_2=\frac{\pi}{4}-\frac{\alpha}{2}} = \frac{\|AB\|\sin(\alpha)}{1+\sin(\alpha)}$,
	$\|OK'\|^*_{\phi_2=\frac{\pi}{4}} = \|AB\|\sin(\alpha)$;

The derivative of $\|OK'\|$ w.r.t. ϕ_2 can be given as follows,

$$\frac{\partial\|OK'\|}{\partial\phi_2} = -\|AB\|\sin(\alpha)\frac{2\cos(2\phi_2)}{\left[\sin(2\phi_2)\right]^2} \tag{B.34}$$

Because of $\phi_2 \geq \frac{\pi}{4}$, $\cos(2\phi_2) \leq 0$ and thus $\frac{\partial\|OK'\|}{\partial\phi_2} \geq 0$. Therefore, if $\|OK'\|$ is the longest distance, the minimum of $\|OK'\|$ is given by

$$\|OK'\|^* = \|OK'\|_{\phi_2=A'(\alpha)} = \frac{\|AB\|\sin(\alpha)}{\sin(2A'(\alpha))}, \quad \alpha \in [0, 0.106\pi]. \tag{B.35}$$

and

$$\|OK'\|^* = \|OK'\|_{\phi_2=\frac{\pi}{4}} = \|AB\|\sin(\alpha), \quad \alpha \in \left[0.106\pi, \frac{\pi}{4}\right]. \tag{B.36}$$

Appendix B.5. Minimize the maximum distance

All the results in Sec. Appendix B.1, Appendix B.2, Appendix B.3, and Appendix B.4 are summarized in Table B.2. By comparing the candidate minimizers in each range of α, the global minimizers are picked up and summarized in Table 1.

Appendix C. Proof of Theorem 3

Assume the distance from the location of the new service node, O, to only one vertex, v^*, equals the longest service distance, denoted by X. We define the set $\mathbb{V}^{(r)}$ including the distances from O to other 4 or 5 vertexes exist in this triangle. We have

$$X > \max\left(\mathbb{V}^{(r)}\right). \tag{C.1}$$

We can always find a direction to move O and reduce $\|Ov^*\|$ by δ_1, and increase $\max\left(\mathbb{V}^{(r)}\right)$ by δ_2. If we further ensure

$$\delta_2 < X - \max\left(\mathbb{V}^{(r)}\right) - \delta_1, \tag{C.2}$$

then the following inequality holds.

$$X - \delta_1 > \max\left(\mathbb{V}^{(r)}\right) + \delta_2. \tag{C.3}$$

Given δ_1 and δ_2 are generated by O's movement, $\delta_2 = 0$ when $\delta_1 = 0$. Considering $X - \max\left(\mathbb{V}^{(r)}\right)$ is positive, we can always satisfy (C.2) by finding a small enough δ_1. Therefore, there is always a movement of O to satisfy (C.3) and further reduce the longest service distance, which means when O is on the optimal location, it cannot have only one vertex as the worst point.

Next, we discuss the case of two vertexes leading to the same longest service distance. There may be a special case where the two worst vertexes and O are in a line. Any movement of O cannot reduce the longest distance. Let us first verify whether it is a possible scenario. Taking Fig. 2 as an example, it is obvious that any two adjacent vertexes cannot be the two worst points. We assume $\angle LOQ = \pi$ and $\|LO\| = \|OQ\|$. It is also easy to find out $\|BL\| = \|QC\|$. Given $\angle ABC \neq \angle ACB$, $\|AB\| \neq \|AC\|$, either $\angle ALQ < \angle ABC$ or $\angle AQL < \angle ACB$ after $\|AB\|$ and $\|AC\|$ are deducted by the same length. For example, $\angle ALQ < \angle ABC$ because of $\alpha > \beta$ in Fig. 2, thus $2\angle LBO < \angle LBO + \phi_2$ and $\angle LBO < \phi_2$. Therefore, we can conclude that, in this case, $\|OK\| = \|BK\| > \|BL\| = \|OL\|$ and L, Q cannot be the only two worst points. If we want to make $\|OL\| = \|ON\|$ and $\angle LON = \pi$, O should move upward because N is above Q, and thus $\|OK\|$ (or possible $\|OK'\|$) further increases. Therefore, L, N cannot be the only two worst points while minimizing the longest service distance. The same method can be applied for M, Q to obtain the same conclusion.

We can easily verify other cases by rotating the triangle. For example, if AC is on the x-axis, by applying the same method above, we can prove that M and P, L and P, M and K cannot be the only two worst points when they are in a line with O, respectively.

If the two worst vertexes and O are not in a line, similarly, we denote the longest service distance as X, the distances from O to the rest vertexes as $\mathbb{V}^{(r)}$. We can always find a direction to move O and reduce the longest service distance by δ_1, and increase $\max\left(\mathbb{V}^{(r)}\right)$ by δ_2. Similar to (C.1)-(C.3) and following analysis, we can prove that if the two worst vertexes and O are not in a line and O is on the optimal location, these two vertexes cannot be the only two worst points.

In summary, any two vertexes cannot be the only two worst points, and thus Theorem 3 is proved.

Appendix D. Supplementary data

Supplementary data to this article can be found online at https://doi.org/10.1016/j.jnca.2019.05.006.

References

3GPP, 2017. Requirements for further advancements for evolved Universal Terrestrial Radio access (E-UTRA) (LTE-Advanced). Release 14, TR 36.913, 3rd Generation Partnership Project (3GPP).

Abo-Zahhad, M., Ahmed, S.M., Sabor, N., Sasaki, S., 2015. Mobile sink-based adaptive immune energy-efficient clustering protocol for improving the lifetime and stability period of wireless sensor networks. IEEE Sens. J. 15, 4576–4586.

Alkesh, A., Singh, A.K., Purohit, N., 2011. A moving base station strategy using fuzzy logic for lifetime enhancement in wireless sensor network. In: International Conference on Communication Systems and Network Technologies, IEEE, pp. 198–202.

Alzenad, M., El-Keyi, A., Lagum, F., Yanikomeroglu, H., 2017. 3D placement of an unmanned aerial vehicle base station (UAV-BS) for energy-efficient maximal coverage. IEEE Wireless Commun. Lett. 6 (4), 434–437.

An, H.-C., Singh, M., Svensson, O., 2017. Lp-based algorithms for capacitated facility location. SIAM J. Comput. 46, 272–306.

Bor-Yaliniz, R.I., El-Keyi, A., Yanikomeroglu, H., 2016. Efficient 3-D placement of an aerial base station in next generation cellular networks. In: International Conference on Communications, IEEE, pp. 1–5.

Chatzigiannakis, I., Kinalis, A., Nikoletseas, S., 2008. Efficient data propagation strategies in wireless sensor networks using a single mobile sink. Comput. Commun. 31, 896–914.

Daniel, K., Wietfeld, C., 2011. Using public network infrastructures for UAV remote sensing in civilian security operations. Homel. Secur. Aff. 7.

FAA, 2016. Docket FAA-2015-0150. Amdt. 107-1, 81 FR 42209.

Gendron, B., Khuong, P.-V., Semet, F., 2017. Comparison of formulations for the two-level uncapacitated facility location problem with single assignment constraints. Comput. Oper. Res. 86, 86–93.

Harris, I., Mumford, C.L., Naim, M.M., 2014. A hybrid multi-objective approach to capacitated facility location with flexible store allocation for green logistics modeling. Transport. Res. E Logist. Transport. Rev. 66, 1–22.

Kalantari, E., Shakir, M.Z., Yanikomeroglu, H., Yongacoglu, A., 2017. Backhaul-aware Robust 3D Drone Placement in 5G Wireless Networks. arXiv preprint arXiv:1702.08395.

Krishnaswamy, R., Sviridenko, M., 2016. Inapproximability of the multilevel uncapacitated facility location problem. ACM Trans. Algorithm 13, 1.

Li, Y., Cai, L., 2017. UAV-assisted dynamic coverage in a heterogeneous cellular system. IEEE Netw. 31, 56–61.

Li, W., Huang, C., Chen, K., Han, S., 2017. A quantitative evaluation method of surveillance coverage of UAVs swarm. In: International Conference on Cloud Computing and Security, Springer, pp. 772–782.

Lilien, L.T., Ben Othmane, L., Angin, P., DeCarlo, A., Salih, R.M., Bhargava, B., 2014. A simulation study of ad hoc networking of uavs with opportunistic resource utilization networks. J. Netw. Comput. Appl. 38, 3–15.

Liu, Z., Chen, Y., Liu, B., Cao, C., Fu, X., 2014. Hawk: An unmanned mini-helicopter-based aerial wireless kit for localization. IEEE Trans. Mob. Comput. 13, 287–298.

Luo, J., Panchard, J., Pirkowski, M., Grossglauser, M., Hubaux, J.-P., 2006. Mobiroute: routing towards a mobile sink for improving lifetime in sensor networks. In: International conference on Distributed Computing in Sensor Systems, Springer, pp. 480–497.

Luo, F., Jiang, C., Du, J., Yuan, J., Ren, Y., Yu, S., Guizani, M., 2015. A distributed gateway selection algorithm for UAV networks. IEEE Trans. Emerging Top. Comput. 3, 22–33.

Mirchandani, P.B., Francis, R.L., 1990. Discrete Location Theory.

Mozaffari, M., Saad, W., Bennis, M., Debbah, M., 2016. Efficient deployment of multiple unmanned aerial vehicles for optimal wireless coverage. IEEE Commun. Lett. 20, 1647–1650.

Mozaffari, M., Saad, W., Bennis, M., Debbah, M., 2016. Unmanned aerial vehicle with underlaid device-to-device communications: performance and tradeoffs. IEEE Trans. Wirel. Commun. 15, 3949–3963.

Mozaffari, M., Saad, W., Bennis, M., Debbah, M., 2016. Mobile internet of Things: can UAVs provide an energy-efficient mobile architecture? In: Global Communications Conference, IEEE, pp. 1–6.

Mozaffari, M., Saad, W., Bennis, M., Debbah, M., 2017. Mobile Unmanned Aerial Vehicles (UAVs) for Energy-Efficient Internet of Things Communications. arXiv preprint arXiv:1703.05401.

Nigam, N., Bieniawski, S., Kroo, I., Vian, J., 2012. Control of multiple UAVs for persistent surveillance: algorithm and flight test results. IEEE Trans. Control Syst. Technol. 20, 1236–1251.

Pan, J., Cai, L., Hou, Y.T., Shi, Y., Shen, S.X., 2005. Optimal base-station locations in two-tiered wireless sensor networks. IEEE Trans. Mob. Comput. 4, 458–473.
Saha, B., Koshimoto, E., Quach, C.C., Hogge, E.F., Strom, T.H., Hill, B.L., Vazquez, S.L., Goebel, K., 2011. Battery Health Management System for Electric UAVs.
Saska, M., Vonsek, V., Chudoba, J., Thomas, J., Loianno, G., Kumar, V., 2016. Swarm distribution and deployment for cooperative surveillance by micro-aerial vehicles. J. Intell. Robot. Syst. 84, 469–492.
Tellier, L.-N., 1972. The weber problem: solution and interpretation. Geogr. Anal. 4, 215–233.
Tellier, L.-N., 1993. conomie spatiale: rationalit conomique de lespace habit. G. Morin, Boucherville, Qubec.
Tuna, G., Nefzi, B., Conte, G., 2014. Unmanned aerial vehicle-aided communications system for disaster recovery. J. Netw. Comput. Appl. 41, 27–36.
Weber, A., 1929. Theory of the Location of Industries. University of Chicago Press.
Xu, X., Luo, J., Zhang, Q., 2010. Delay tolerant event collection in sensor networks with mobile sink. In: International Conference on Computer Communications, IEEE, pp. 1–9.
Yun, Y., Xia, Y., 2010. Maximizing the lifetime of wireless sensor networks with mobile sink in delay-tolerant applications. IEEE Trans. Mob. Comput. 9, 1308–1318.
Zorbas, D., Pugliese, L.D.P., Razafindralambo, T., Guerriero, F., 2016. Optimal drone placement and cost-efficient target coverage. J. Netw. Comput. Appl. 75, 16–31.

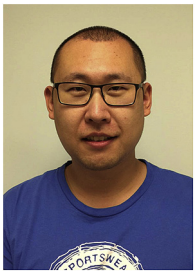

Yue Li received his Ph.D. degree in electrical and computer engineering from the University of Victoria, Victoria, Canada, in 2018. During 2008–2013, he worked for Huawei as a standard pre-research engineer in the Wireless Research Department. He has been closely involved in 3GPP standards evolvement and held numerous patents in WCMDA, LTE-A, and 5G systems. Currently, he is a Postdoctoral Research Fellow in the Department of Electrical and Computer Engineering, University of Victoria, Victoria, Canada. His research interests include next-generation cellular system, wireless network design and optimization, wireless system modeling and performance analysis.

Yongmin Zhang (S′12-M′15) received the Ph.D. degree in control science and engineering from Zhejiang University, Hangzhou, China, in 2015. He is currently a Postdoctoral Research Fellow in both the State Key Laboratory of Industrial Control Technology at Zhejiang University and the Department of Electrical and Computer Engineering, University of Victoria, Victoria, BC, Canada. His research interests include wireless sensor networks, resource management and optimization, and smart grid.

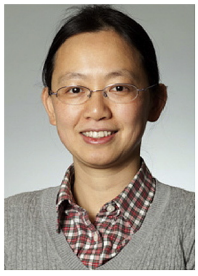

Lin Cai (S′00-M′06-SM′10) received her M.A.Sc. and Ph.D. degrees in electrical and computer engineering from the University of Waterloo, Waterloo, Canada, in 2002 and 2005, respectively. Since 2005, she has been with the Department of Electrical & Computer Engineering at the University of Victoria, and she is currently a Professor. Her research interests span several areas in communications and networking, with a focus on network protocol and architecture design supporting emerging multimedia traffic over wireless, mobile, ad hoc, and sensor networks. She has served as a TPC symposium co-chair for IEEE Globecom'10 and Globecom'13. She served as an Area Editor of the IEEE Transactions on Vehicular Technology, an Associate Editor of the IEEE Transactions on Wireless Communications, IEEE Transactions on Vehicular Technology, EURASIP Journal on Wireless Communications and Networking, International Journal of Sensor Networks, and Journal of Communications and Networks (JCN), and as the Distinguished Lecturer of the IEEE VTS Society. She was a recipient of the NSERC Discovery Accelerator Supplement Grants in 2010 and 2015, respectively, the NSERC E.W.R. Steacie Memorial Fellowship in 2019, and the Best Paper Awards of IEEE ICC 2008 and IEEE WCNC 2011. She has founded and co-chaired IEEE Victoria Section Vehicular Technology and Communications Joint Societies Chapter.